Letter

First-principles study of recombination-enhanced migration of an interstitial magnesium in gallium nitride

Yuansheng Zhao [1,*] Kenji Shiraishi [1,2] Tetsuo Narita,[3] and Atsushi Oshiyama[1]
[1]*Institute of Materials and Systems for Sustainability, Nagoya University, Nagoya 464-8603, Japan*
[2]*Graduate School of Engineering, Nagoya University, Nagoya 464-8601, Japan*
[3]*Toyota Central R&D Laboratories, Inc., Nagakute, Aichi 480-1192, Japan*

(Received 2 May 2024; revised 28 June 2024; accepted 31 July 2024; published 16 August 2024)

The stable and metastable configurations of interstitial Mg in GaN and its migration energy barriers are studied from first-principles calculations. In addition to the conventional octahedral (O, global energy minimum) and tetrahedral (T, metastable) interstitial sites, we have discovered two metastable interstitial complexes with formation energy lower than or close to that of the T configuration but higher than O. Except for Mg at O site, which only has +2 charge state, all other configurations also permit charge states +1 or 0. The minimum migration energy barrier for Mg^{++} between O sites is found to be 1.95 eV. We further find that, when Fermi energy is close to the conduction band, the migration between O sites via metastable configurations occurs through a recombination-enhanced mechanism in which the charge state changes from +2 at O site to 0 at metastable sites by consecutive capture of two electrons during the migration. This process greatly reduces the migration energy barrier to as low as 1.47 eV. This value is consistent with experiments, and we also discuss the role of intrinsic defects in the migration of Mg.

DOI: 10.1103/PhysRevB.110.L081201

Doping of donor and acceptor impurities, which generate electrons and holes carrying electric currents, is essential in the fabrication of electronic devices, making it a central issue in semiconductor science and technology [1–3]. The doping can be fulfilled during epitaxial growth of semiconductor thin films. However, to achieve the desired profiles of donors and acceptors in complicated device structures, ion implantation followed by thermal annealing is indispensable. During such doping processes, atomic diffusion and migration are key phenomena that govern the profiles of donor and acceptor concentrations.

Gallium nitride (GaN) is a premier semiconductor in optoelectronics and is promising for advancing future power electronics. In GaN, an Mg atom substitutes for the Ga site and functions exclusively as an acceptor. In the fabrication of planar optical devices, the Mg has been usually doped during the epitaxial growth of GaN [4–6]. In the case of power devices, however, Mg doping via the ion implantation technique is necessary but has not been achieved before because of N desorption during annealing. Recently, Sakurai and collaborators at Nagoya University have succeeded in fabricating *p*-type GaN through Mg implantation followed by annealing under high pressure of nitrogen [7,8], advancing the doping technology in GaN to a next stage comparable to the Si technology. At this point, unveiling the migration mechanism of an interstitial Mg atom, which is generated during the implantation process in GaN becomes crucial.

Atomistic knowledge as to the Mg migration in GaN is surprisingly poor. The only *ab initio* study is done by Miceli and Pasquarello [9]. They have performed microscopic calculations based on the density functional theory (DFT) [10,11] with generalized gradient approximation (GGA) [12], assuming that the diffusing species is doubly positive magnesium (Mg^{++}). They have identified two (meta)stable interstitial sites, the octahedral (O) and tetrahedral (T) sites for Mg^{++}, and found three distinct pathways in the interstitial channels. The calculated migration barrier is more than 2 eV. Experimentally, the measured values for the migration or diffusion barriers vary widely [13–18]. An earlier study reported a low barrier of 1.3 eV for vapor phase diffusion in *n*-type GaN [13], whereas another study reported a value of 1.9 eV [14]; recently, the barrier of interstitial migration is estimated to be $1.3 \sim 2.3$ eV from β^- emission channeling [15,16]. This diversity of the experimental value is presumably the result of the differences in experimental situations such as characteristics of samples, device structures, etc. Therefore, a direct comparison of the calculated migration barrier with the experimental values is not straightforward. However, it is certain that there are experimentally reported barriers lower than the calculated barrier for the Mg^{++} migration. This observation infers the existence of unidentified processes with higher hopping rates than that in simple Mg^{++} migration. Moreover, it is reported that the diffusion of Mg in GaN is suppressed when annealing under high-pressure N_2 [19]. This implies that the Mg-migration barrier is affected by N-related intrinsic defects such as N vacancies, which are considered to work as donor-type defects [20,21].

In this Letter, we report first-principles calculations based on DFT for the interstitial Mg in GaN and find that, in addition to Mg^{++}, other charge states Mg^{+} and Mg^{0} appear during the migration. This variation of the charge states reduces the

*Contact author: zhao.yuansheng.u3@f.mail.nagoya-u.ac.jp

migration barrier by around 0.5 eV (recombination-enhanced migration), thus providing a possible mechanism for the low barrier as stated above. We also find metastable complexes of Mg and Ga in the interstitial region, which enrich the migration pathways. Roles of intrinsic defects presumably generated during the ion implantation for the Mg migration are also discussed.

First-principles DFT calculations have been performed with the VASP package [22,23] using the projector-augmented potentials [24] with Ga $3d$ states in the core. We use GGA [12] for the exchange-correlation energy during the geometry optimization, and then employ hybrid approximation (HSE) [25] to calculate the electronic structures and total energies accurately for optimized geometries [26]. We set the cutoff energy of 400 eV for the plane-wave basis and use the calculated values for lattice constants (wurtzite phase) $a = 3.23$ Å and $c = 5.25$ Å, which agree with the experimental values with an error of ∼1%. The calculated band gap of crystalline GaN is 3.4 eV in the present hybrid approximation with the mixing parameter $\alpha = 0.34$ of Fock exchange. An Mg interstitial is embedded in a 4×4×3 supercell (192 atoms without defect) and is optimized using 2×2×2 $\boldsymbol{k}$-point mesh until the force acting on each atom is smaller than 0.01 eV Å^{-1}. The migration path is explored by the nudged elastic band (NEB) method with improved tangential estimate [27]. Here, the minimum energy path (i.e. the migration coordinate ξ) between the initial and final (meta)stable geometries in the multidimensional space of atomic coordinates is approximated by several intermediate geometries called *images* obtained by constraint total-energy minimization. Further details of the present calculations are found within the Supplemental Material (SM) [28].

The formation energy of each geometric configuration of Mg-related defects (labelled as ζ below) with charge state q is computed as

$$\Delta E_\zeta(q) = E_\zeta(q) - \left(E_{\rm ref} + \sum_i \Delta N_i \mu_i\right) + q(E_{\rm VBT} + E_{\rm F}) + E_{\rm corr}(q). \quad (1)$$

Here, $E_\zeta(q)$ and $E_{\rm ref}$ are the total energies of the supercell models for the Mg interstitial and the reference structure (taken as a perfect GaN supercell), respectively; μ_i and ΔN_i are the chemical potential of the element i and its difference in number from the reference structure, respectively; $E_{\rm VBT}$ and $E_{\rm F}$ are the energy of valence band top (VBT) and Fermi-level position relative to VBT, respectively; $E_{\rm corr}(q)$ is the correction term for charge state q because of the finite size of the supercell model [29].

We set out with stable and metastable geometric configurations of an interstitial Mg in GaN by an extensive search with GGA calculations. In wurtzite structure, there are typical interstitial sites: i.e., the octahedral (O) and tetrahedral (T) sites surrounded by the octahedrons and the tetrahedrons, respectively, consisting of either Ga or N atoms. The two Ga or N octahedrons (tetrahedrons) are slightly shifted to each other. Previous DFT calculations [9] examined their stability for doubly positive Mg. We have also examined the stability of Mg^{++} at the O and T sites and found that both sites are stable although Mg is slightly dislodged from the high-symmetry

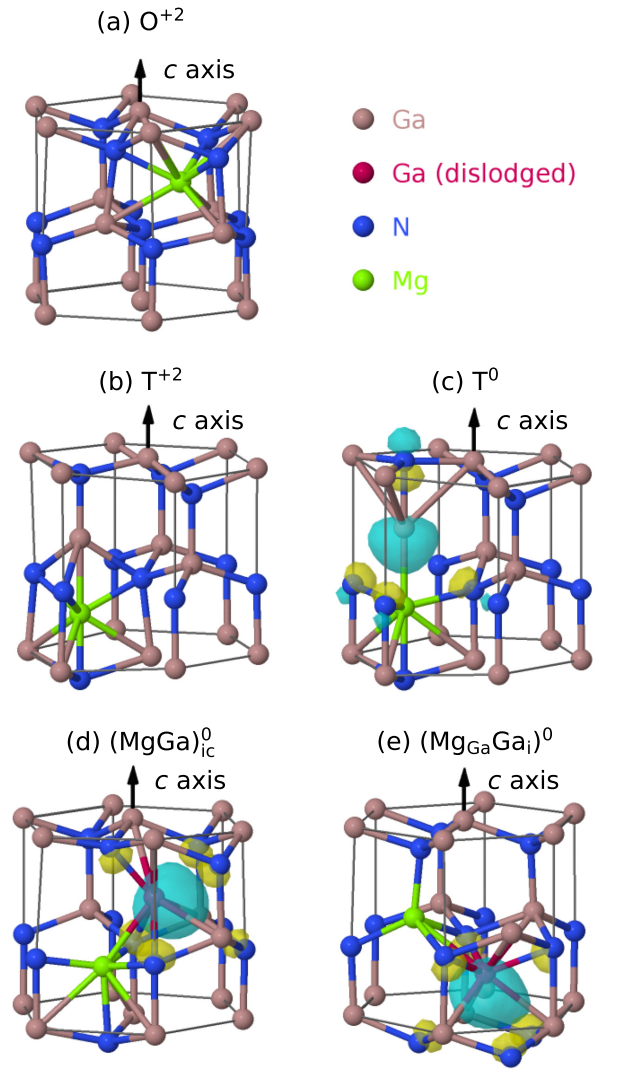

FIG. 1. Stable and metastable configurations of interstitial Mg in GaN: (a) O^{+2}, (b) T^{+2}, (c) T^0, (d) $(MgGa)^0_{ic}$, and (e) $(Mg_{Ga}Ga_i)^0$ configurations. The superscripts denote the charge state. For the last three structures, the wavefunction of the gap state is also shown.

points in both cases, as shown in Figs. 1(a) and 1(b) and Table SI within the SM [28]. The O site is lower in the formation energy than the T site by 2.10 eV, which agrees well with the previous result [9]. We have also examined charge states other than doubly positive. At the O site we have found that +2 is the only possible charge state. This is because Mg at the O site induces no gap state so that two additional valence electrons of Mg are missing for any position of the $E_{\rm F}$ in the gap. In contrast, we have found that Mg at the T site becomes neutral when $E_{\rm F}$ is near to the conduction band bottom (CBB), as is shown in Fig. 2. The formation energy is reduced by 1.13 eV with $Mg^{++}_{\rm T}$ becoming $Mg^0_{\rm T}$ when $E_{\rm F}$ is at CBB. The appearance of the neutral charge state at the T site is associated with substantial relaxation of surrounding atoms, which induces the mid gap state [Fig. 1(c)]. Providing a single electron is not enough to attain such configuration. We have indeed found that the singly positive-charged Mg at the T site is unstable.

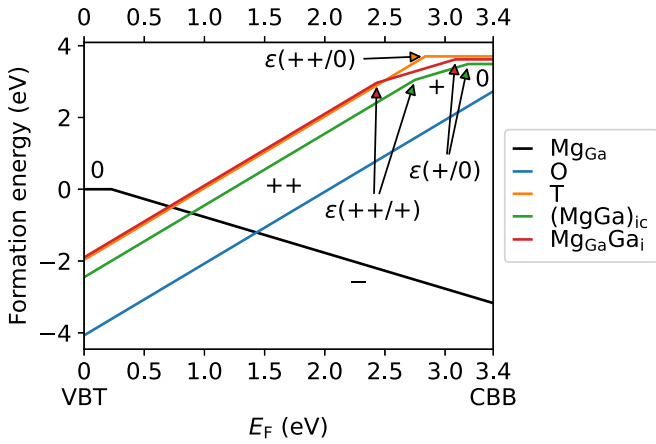

FIG. 2. Formation energy of the interstitial Mg at various sites and with various charge states q as a function of the Fermi-level position in the gap relative to that of the neutral substitutional Mg, Mg_{Ga}, under Ga-rich condition (i.e., μ_{Ga} = energy of Ga metal). The thermodynamic level $\varepsilon(q/q')$ is determined by the cross point of the formation energies with q and q'.

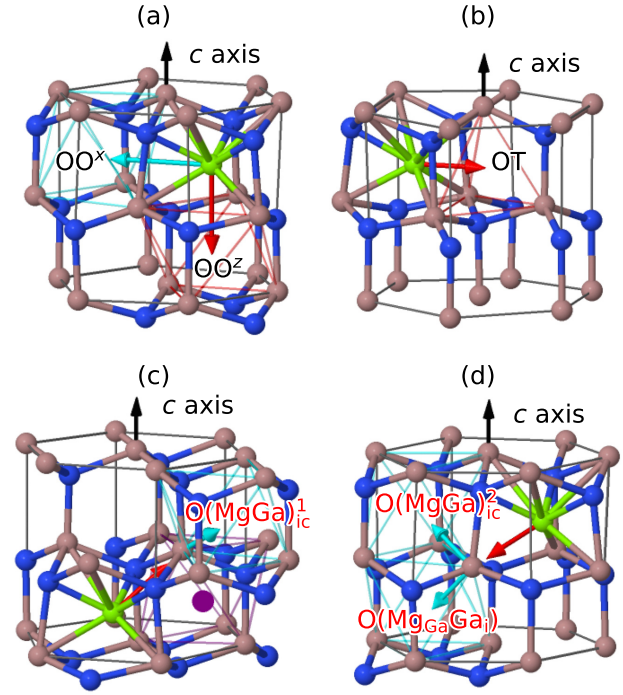

FIG. 3. (a) OO^z and OO^x paths; (b) OT path; (c) $O(MgGa)^1_{ic}$ path, the red and light blue arrows show the movement of Mg and Ga, respectively. The purple dot shows a possible final position of Mg after completing this pathway followed by its reverse; and (d) $O(MgGa)^2_{ic}$ path and $O(Mg_{Ga}Ga_i)$ path, the movement of Mg is the same in these two paths.

In addition to the Mg at the O and T sites, we have found two other metastable configurations, which have never been addressed before: One is an interstitial complex $(MgGa)_{ic}$, a kind of "split interstitial", where Mg and dislodged Ga are located near a single lattice site with $\overrightarrow{MgGa}$ direction approximately parallel to $[4\bar{4}05]$, and the other is a pair of substitutional Mg and an interstitial Ga near the O site $Mg_{Ga}Ga_i$, as shown in Figs. 1(d) and 1(e), respectively. It is found that for both structures, the Mg and dislodged Ga both lie in $(1\bar{1}00)$ plane (Fig. S1 within the SM [28]). For doubly positive-charge state, the formation energies of $(MgGa)_{ic}$ and $Mg_{Ga}Ga_i$ are comparable with that at the T site (Fig. 2). The $(MgGa)_{ic}$ is actually found to be even lower than the T. More importantly, those configurations induce gap states, which can capture electrons, thus rendering the +1 and neutral states realized. As shown in Fig. 2, the +1 and neutral $(MgGa)_{ic}$ and $Mg_{Ga}Ga_i$ appear when the E_F is close to CBB. Yet, we have found that, unlike the T configuration, the local structures are essentially the same for different charge states.

Several metastable configurations with distinct charge state we have found here open a possibility of carrier recombined migration of the interstitial Mg, in particular when E_F is close to CBB. The charge states other than +2 for Mg interstitial have never been discussed before. As shown in Fig. 2, Mg_{Ga} is the most stable form of Mg for a wide range of the Fermi-level position and acts as an acceptor evidenced by the appearance of the thermodynamic level $\varepsilon(0/-)$ near VBT. Thus, in the equilibrium condition, Mg-doped GaN is expected to be p type. However, in Mg doping through the ion implantation, which is an indispensable fabrication technique of electronic devices, nonequilibrium conditions are common. In this case, the interstitial Mg and other intrinsic defects become abundant. Figure 2 shows that the interstitial Mg may act as a donor or a double donor. In addition, previous DFT calculations [20,21] show that N vacancy and Ga interstitial induce donor-type gap levels. Because the excess Mg cation is introduced, these two types of defects are expected to form relatively easily. Under these considerations, it is possible for the Fermi-level position to be raised to near the conduction band and thus the metastable configurations with $q = +1$ or 0 of interstitial Mg can become active.

From the calculated formation energies, the interstitial Mg at the O site with +2 charge state is energetically most favorable irrespective of the E_F position. Hence, the movement from one O site to a neighboring equivalent O site is the elementary process of the migration of the interstitial Mg. We have explored pathways for such elementary processes through NEB calculations. In the simplest pathways, as shown in Fig. 3(a), the Mg at an O site can migrate directly to nearby O site in z direction (c axis) or xy plane without passing through any metastable sites. We refer to these two pathways as OO^z and OO^x, respectively. Clearly, the migration from an O site to one of the metastable sites and then to neighboring O site is also possible. Due to structural symmetry, it suffices to examine half of the pathways, i.e., the pathways between O and metastable sites. We have found four such pathways, as shown in Figs. 3(b)–3(d). In the OT pathway, the Mg simply moves in xy plane and migrates to a neighboring T site [Fig. 3(b)]. Regarding the pathways to $(MgGa)_{ic}$ or $Mg_{Ga}Ga_i$, we have found two distinct processes, $O(MgGa)^1_{ic}$ and $O(MgGa)^2_{ic}$ (the superscripts denote the labels of pathways) where the moving directions of Mg are different as shown in Figs. 3(c) and 3(d), and a single process $O(Mg_{Ga}Ga_i)$ [Fig. 3(d)]. In these processes, the Mg at the O site moves towards one of the neighboring Ga atoms (red arrows in the figure) and pushes it to a nearby interstitial O

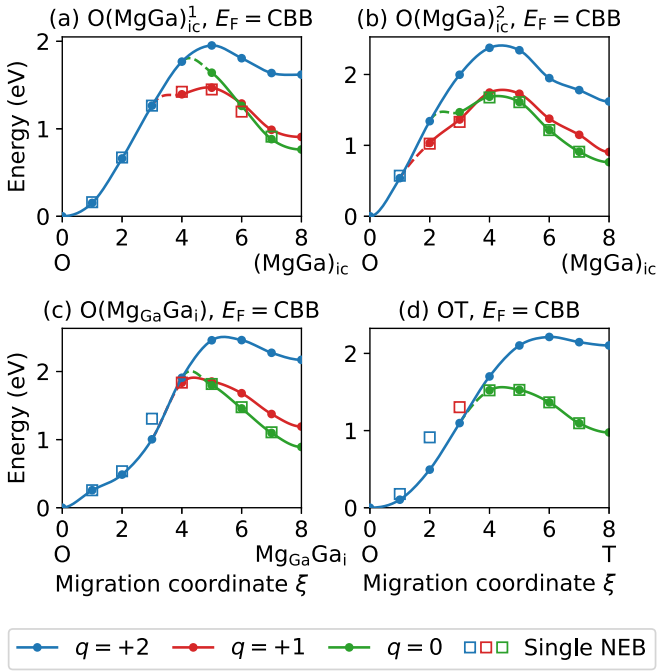

FIG. 4. Total energy profiles along the four distinct migration pathways, (a) O(MgGa)$^1_{ic}$, (b) O(MgGa)$^2_{ic}$, (c) O(Mg$_{Ga}$Ga$_i$), and (d) OT. The energy profile along each pathway is shown for +2 (blue), +1 (red), and neutral (green) charge states (kept fixed during the whole migration). The squares are the results of a single calculation with varying charge states along the migration path. The abscissa is the migration coordinate ξ representing a particular intermediate structure in multidimensional atomic coordinates along the migration path. Relative energy positions among different charge states depend on the Fermi-level (E_F) position and in this figure E_F is set to be at the conduction band bottom.

site (light blue arrows) to form (MgGa)$_{ic}$ or Mg$_{Ga}$Ga$_i$ configuration. We emphasize that from the metastable sites, the Mg can go to *another* nearby O site with the same energy barrier and continue to migrate. For example, the O(MgGa)$^1_{ic}$ process followed by its reverse process (MgGa)$_{ic}$O^1 can send the Mg to a neighboring O site, as is shown by the purple dot in Fig. 3(c), thus the combined processes are equivalent to an OO^x process. Note that, although the Mg may also go back to the original O site in the reverse process, this kind of reversibility does not negate the diffusion (actually it is common for all diffusion processes). The important point is that the Mg can diffuse arbitrarily far away given a sufficient number of hopping steps along these pathways. In this way, the Mg movement between the O site and the metastable configuration effectively contributes to the Mg migration between the most stable O sites.

After identifying the migration pathways described above, we have obtained the energy profiles along the pathways by HSE calculations. At first, we have calculated the energy profiles along the OO^z, OO^x (not shown), and OT [Fig. 4(d)] pathways for Mg^{++}. The obtained profiles are similar to those reported in the previous paper [9]. The calculated migration barriers are 2.02, 1.95, and 2.21 eV for the OO^z, OO^x, and OT, respectively in the present calculations, which are close to the previous values, 2.01, 2.19, and 2.20 eV. Only for the OO^x, the values are different by 0.24 eV (10%). This discrepancy could be attributed to the different pseudopotentials used (PAW in this paper vs norm-conserving in Ref. [9]) or the stricter convergence criterion in our calculation (0.01 vs 0.05 eV/Å), which is necessary to determine the transition-state geometry in the plateau-like energy landscape in this case.

TABLE I. Migration barrier (eV) of each pathway at E_F = VBT and CBB.

Pathways	$E_a(E_F = \text{VBT})$	$E_a(E_F = \text{CBB})$
OO^z	2.02	2.02
OO^x	**1.95**	1.95
OT	2.21	1.56
O(MgGa)$^1_{ic}$	**1.95**	**1.47**
O(MgGa)$^2_{ic}$	2.41	1.70
O(Mg$_{Ga}$Ga$_i$)	2.51	1.91

The calculated energy profiles along the pathways from O sites to metastable configurations, (MgGa)$_{ic}$, Mg$_{Ga}$Ga$_i$ and the T sites, are shown for Mg^{++} in Fig. 4 as a function of the migration coordinate ξ. As stated in the method part, the coordinate ξ represents a particular intermediate structure in multidimensional atomic coordinates along each migration pathway. Among all pathways for Mg^{++}, we have found that the minimum migration energy barrier between O sites is 1.95 eV and achieved in the OO^x and O(MgGa)$^1_{ic}$ pathways (Table I). While the obtained minimum value is lower than the previous value by 10%, the migration barrier is still too large to explain the possibly very low values found in some experiments.

As discussed above, the metastable configurations induce gap states and thus take different charge states, +1 and neutral. We have found that this is also true for the intermediate geometries along the pathways. This finding brings forth a possibility of the migration in which the charge state is varying (recombination enhanced/retarded migration). When E_F is close to CBB, the +1 and the neutral metastable states are energetically favorable (Fig. 2) and thus the recombination enhanced migration is expected to be important.

To verify this, we have performed a series of NEB calculations with all three charge states. Let us focus on the migration through the O(MgGa)$^1_{ic}$ pathway [Fig. 4(a)], in which the migration barrier for Mg^{++} is the lowest, 1.95 eV. The results from the NEB calculations with $q = +1$ and 0 are also shown in Fig. 4(a). When the Mg starts to migrate ($\xi \leqslant 3$), the only possible charge state is $q = +2$ (no gap state). As Mg proceeds ($\xi \geqslant 4$), the gap state appears and the charge can become $q = +1$ with much reduced formation energy than $q = +2$. Near the transition state for the Mg^{++} migration ($\xi \approx 5$), the gap state can accommodate two electrons and $q = 0$ is also available. The relative energies for different charge states depend on the E_F position, as is demonstrated in Fig. 2. Figure 4 shows the results when E_F is at CBB. In this case, the present calculations have unequivocally clarified that Mg starts at the O site as the +2 charge state, successively captures the first and then the second electrons to lower its energy, with the charge state being changed to +1 then

neutral, and reaches the $(MgGa)_{ic}$ configuration. The calculated migration barrier is 1.47 eV and the electron capture substantially reduces the migration barrier.

The recombination-enhanced Mg migration clarified above relies on the ansatz that the lowest-energy charge state is reached during the migration. This is generally true since the ionic motion is much slower than the electronic transition. Yet, a particular charge state of defects can be long lived in semiconductors, e.g., DX center in compound semiconductors [30]. This is usually associated with structural reconstruction between distinct charge states, where an energy barrier exists. In the present calculations, this is already taken into account in the DFT-NEB scheme since there is no abrupt structural changes along the migration pathways. Another important factor is the peculiar electronic structure of the interstitial Mg. It generally induces localized electron states in the band gap near CBB consisting mainly of Ga and N atomic orbitals nearby as shown in Fig. 1. However, at the O site, the interstitial Mg induces no localized gap states but resonant states in the conduction (and also valence) bands. This is presumably caused by the high symmetry at the O-site geometry, as in the tetrahedral interstitial site in Si [31,32]. As a result, at the O site, Mg becomes $q = +2$ with two valence electrons transferred to the conduction band. Then during the migration towards other metastable geometries with the lower symmetry, we have found that the resonant state shifts downward and emerges in the gap, being ready to capture electrons, especially near the crossing point. No particular energy barriers emerge upon the electron capture, as discussed above.

However, the above NEB calculations with distinct charge states do not include the possible energy barrier resulting from the slightly different local structures of distinct charge states at the same ξ. To clarify this issue, we perform another single NEB calculation connecting the Mg_O^{++} and $(MgGa)_{ic}^{0}$ structures by setting $q = +2$, $+1$, and 0 for images $\xi \leqslant 3$, $4 \leqslant \xi \leqslant 6$ and $\xi = 7$, respectively. In this way, the structural change along the migration path becomes fully "continuous". The energy profile obtained by this single NEB is shown by the empty squares in Fig. 4(a). It is found that the energy profile is slightly different among distinct NEB calculations because of local relaxation at different q, but the overall energy barriers are essentially identical.

When E_F is lowered by $\Delta\epsilon$ from CBB, the energy profiles for $q = +1$ and 0 along the migration pathways are shifted upwards by $\Delta\epsilon$ and $2\Delta\epsilon$, respectively, relative to the energy for $q = +2$, as is derived from Eq. (1), leading to the increase of the migration barrier. The migration barrier $E_a(E_F)$ at arbitrary E_F position in the gap is calculated from the computed results described above. For each pathway, it is

$$E_a(E_F) = \max_{\xi} \left\{ \min_{q\in\{+2,+1,0\}} E_q(\xi, E_F) \right\}.$$

Here $E_q(\xi, E_F)$ is the formation energy of the intermediate structure ξ with the charge state q at E_F. The result for the $O(MgGa)_{ic}^{1}$ pathway is shown by the blue line in Fig. 5 and we observe a linear decrease of the migration barrier for E_F above VBT + 2.9 eV.

We have performed the same calculations for other pathways, the $O(MgGa)_{ic}^{2}$, $O(Mg_{Ga}Ga_i)$, and OT. The results are shown in Figs. 4(b)–4(d) and Fig. 5. The Mg migration along those pathways is found to exhibit similar behavior as in the

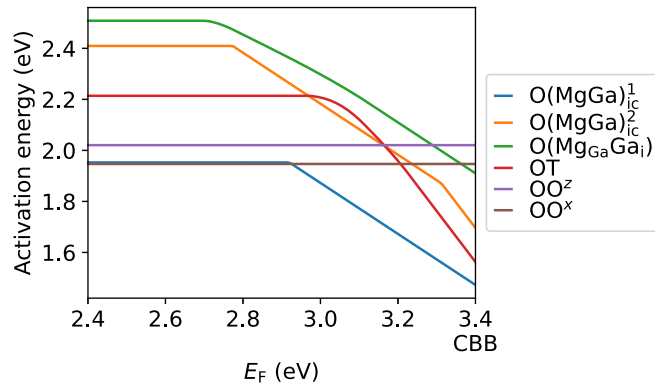

FIG. 5. The migration barriers as a function of the Fermi-level position in the gap for distinct migration pathways. All energy barriers are constant below CBB − 1 eV.

$O(MgGa)_{ic}^{1}$ pathway: i.e., the migration barrier is reduced with increasing E_F because of the recombination enhanced migration. In the case of OT path, although $q = +1$ does not exist at T, we find that the Mg still captures the electrons consecutively similar to other pathways and $q = +1$ is the most stable at intermediate structure $\xi = 3$ (indicated by the colors of empty squares in Fig. 4).

For direct migration through the OO^z and OO^x pathways, no gap state appears during the migration and the recombination enhancement of the migration is not observed (not shown in Fig. 4). The migration barriers are unaffected by the E_F position (Fig. 5).

We summarize the energy barrier for each pathway at E_F = VBT and CBB in Table I. At high Fermi level, the lowest energy barrier for migration between O sites is 1.47 eV, almost 0.5 eV lower than that for low Fermi level. There are also multiple pathways with energy barriers well below 2 eV, agreeing with the values obtained from experiments. By considering the intrinsic defects, we can also provide a possible explanation for the slowdown of the Mg migration by high N_2 pressure [19] as mentioned earlier: The N vacancies in GaN can act as electron donors [20,21] and raise the Fermi level position, assisting the migration of Mg. Under high N_2 ambient pressure, the concentration of the N vacancy decreases, and the Mg migration is then suppressed by the E_F lowering.

In conclusion, we have studied the structure of Mg interstitial in GaN and migration pathways and barriers between the (meta)stable configurations from *ab initio* calculations. In addition to previously reported O and T sites, we have discovered two configurations $(MgGa)_{ic}$ and $Mg_{Ga}Ga_i$ with formation energy lower than or close to that of T configuration. Except for Mg at O site, which only has +2 charge state, all other configurations also admit charge states +1 and 0. For low Fermi level, the minimum migration energy barrier for Mg^{++} between O sites is 1.95 eV. When Fermi energy is close to CBB, the migration via metastable configurations occurs through the recombination-enhanced mechanism. The charge state changes from +2 at O site to 0 at metastable sites by capturing two electrons successively during the migration. This process greatly reduces the migration energy barrier and the minimum energy barrier is reduced to as low as 1.47 eV for E_F at CBB, a value consistent with experiments.

The data that support the findings of this study are available from the corresponding author upon reasonable request.

This work is supported by the Ministry of Education, Culture, Sports, Science and Technology (MEXT) programs "Creation of innovative core technology for power electronics" (Grant No. JPJ009777), as well as Grant-in-Aid (Kakenhi) for Japan Society for the Promotion of Science (JSPS) Fellows No. 22KJ0579. The computation in this work has been done using the facilities of the Supercomputer Center, the Institute for Solid State Physics, the University of Tokyo.

[1] S. M. Sze, Y. Li, and K. K. Ng, *Physics of Semiconductor Devices* (John Wiley & Sons, Hoboken, NJ, 2021).

[2] T. Narita and T. Kachi, *Characterization of Defects and Deep Levels for GaN Power Devices* (AIP Publishing, Melville, New York, 2020).

[3] S. T. Pantelides, The electronic structure of impurities and other point defects in semiconductors, Rev. Mod. Phys. **50**, 797 (1978).

[4] I. Akasaki, Nobel lecture: Fascinated journeys into blue light, Rev. Mod. Phys. **87**, 1119 (2015).

[5] H. Amano, Nobel lecture: Growth of GaN on sapphire via low-temperature deposited buffer layer and realization of *p*-type GaN by Mg doping followed by low-energy electron beam irradiation, Rev. Mod. Phys. **87**, 1133 (2015).

[6] S. Nakamura, Nobel lecture: Background story of the invention of efficient blue InGaN light emitting diodes, Rev. Mod. Phys. **87**, 1139 (2015).

[7] H. Sakurai, M. Omori, S. Yamada, Y. Furukawa, H. Suzuki, T. Narita, K. Kataoka, M. Horita, M. Bockowski, J. Suda, and T. Kachi, Highly effective activation of Mg-implanted *p*-type GaN by ultra-high-pressure annealing, Appl. Phys. Lett. **115**, 142104 (2019).

[8] H. Sakurai, T. Narita, M. Omori, S. Yamada, A. Koura, M. Iwinska, K. Kataoka, M. Horita, N. Ikarashi, M. Bockowski, J. Suda, and T. Kachi, Redistribution of Mg and H atoms in Mg-implanted GaN through ultra-high-pressure annealing, Appl. Phys. Express **13**, 086501 (2020).

[9] G. Miceli and A. Pasquarello, Migration of Mg and other interstitial metal dopants in GaN, Phys. Status Solidi RRL **11**, 1700081 (2017).

[10] P. Hohenberg and W. Kohn, Inhomogeneous electron gas, Phys. Rev. **136**, B864 (1964).

[11] W. Kohn and L. J. Sham, Self-consistent equations including exchange and correlation effects, Phys. Rev. **140**, A1133 (1965).

[12] J. P. Perdew, K. Burke, and M. Ernzerhof, Generalized gradient approximation made simple, Phys. Rev. Lett. **77**, 3865 (1996).

[13] C. Pan and G. Chi, The doping of GaN with Mg diffusion, Solid-State Electron. **43**, 621 (1999).

[14] Z. Benzarti, I. Halidou, Z. Bougrioua, T. Boufaden, and B. El Jani, Magnesium diffusion profile in GaN grown by MOVPE, J. Cryst. Growth **310**, 3274 (2008).

[15] U. Wahl, L. M. Amorim, V. Augustyns, A. Costa, E. David-Bosne, T. A. L. Lima, G. Lippertz, J. G. Correia, M. R. da Silva, M. J. Kappers, K. Temst, A. Vantomme, and L. M. C. Pereir, Lattice location of Mg in GaN: A fresh look at doping limitations, Phys. Rev. Lett. **118**, 095501 (2017).

[16] U. Wahl, J. G. Correia, A. R. Costa, E. David-Bosne, M. J. Kappers, M. R. da Silva, G. Lippertz, T. A. Lima, R. Villarreal, A. Vantomme, and L. M. Pereira, Lattice location studies of the amphoteric nature of implanted Mg in GaN, Adv. Electron. Mater. **7**, 2100345 (2021).

[17] S. Porowski, I. Grzegory, D. Kolesnikov, W. Lojkowski, V. Jager, W. Jager, V. Bogdanov, T. Suski, and S. Krukowski, Annealing of GaN under high pressure of nitrogen, J. Phys.: Condens. Matter **14**, 11097 (2002).

[18] Y. Itoh, S. Lu, H. Watanabe, M. Deki, S. Nitta, Y. Honda, A. Tanaka, and H. Amano, Substitutional diffusion of Mg into GaN from GaN/Mg mixture, Appl. Phys. Express **15**, 116505 (2022).

[19] K. Sumida, K. Hirukawa, H. Sakurai, K. Sierakowski, M. Horita, M. Bockowski, T. Kachi, and J. Suda, Effect of annealing time and pressure on electrical activation and surface morphology of Mg-implanted GaN annealed at 1300 Â°C in ultra-high-pressure nitrogen ambient, Appl. Phys. Express **14**, 121004 (2021).

[20] J. L. Lyons and C. G. Van de Walle, Computationally predicted energies and properties of defects in GaN, npj Comput. Mater. **3**, 12 (2017).

[21] G. Miceli and A. Pasquarello, Self-compensation due to point defects in Mg-doped GaN, Phys. Rev. B **93**, 165207 (2016).

[22] G. Kresse and J. Furthmüller, Efficient iterative schemes for *ab initio* total-energy calculations using a plane-wave basis set, Phys. Rev. B **54**, 11169 (1996).

[23] G. Kresse and D. Joubert, From ultrasoft pseudopotentials to the projector augmented-wave method, Phys. Rev. B **59**, 1758 (1999).

[24] P. E. Blöchl, Projector augmented-wave method, Phys. Rev. B **50**, 17953 (1994).

[25] J. Heyd, G. E. Scuseria, and M. Ernzerhof, Hybrid functionals based on a screened Coulomb potential, J. Chem. Phys. **118**, 8207 (2003).

[26] We have tested that including the 3*d* electrons in the valence states or using HSE rather than GGA for the energy minimization changes the formation energy of Mg-related defects typically by less than 0.1 eV.

[27] G. Henkelman and H. Jónsson, Improved tangent estimate in the nudged elastic band method for finding minimum energy paths and saddle points, J. Chem. Phys. **113**, 9978 (2000).

[28] See Supplemental Material at http://link.aps.org/supplemental/10.1103/PhysRevB.110.L081201 for details of the calculations, and additional figures and tables.

[29] C. Freysoldt, J. Neugebauer, and C. G. Van de Walle, Fully *ab initio* finite-size corrections for charged-defect supercell calculations, Phys. Rev. Lett. **102**, 016402 (2009).

[30] P. Mooney, Deep donor levels (DX centers) in III-V semiconductors, J. Appl. Phys. **67**, R1 (1990).

[31] R. Car, P. J. Kelly, A. Oshiyama, and S. T. Pantelides, Microscopic theory of atomic diffusion mechanisms in silicon, Phys. Rev. Lett. **52**, 1814 (1984).

[32] G. A. Baraff, M. Schluter, and G. Allan, Theory of enhanced migration of interstitial aluminum in silicon, Phys. Rev. Lett. **50**, 739 (1983).